Journal of Alloys and Compounds 508 (2010) 592–598

Contents lists available at ScienceDirect

Journal of Alloys and Compounds

journal homepage: www.elsevier.com/locate/jallcom

Mechanisms of improving the cyclic stability of V–Ti-based hydrogen storage electrode alloys

He Miao*, Wei Guo Wang

Division of Fuel Cell and Energy Technology, Ningbo Institute of Materials Technology & Engineering, Chinese Academy of Sciences, Ningbo 315201, PR China

ARTICLE INFO

Article history:
Received 10 July 2010
Received in revised form 19 August 2010
Accepted 25 August 2010
Available online 24 September 2010

Keywords:
V–Ti-based alloys
Hydrogen storage electrode alloys
Cyclic stability
Pulverization

ABSTRACT

In this work, the mechanisms of improving the cyclic stability of V–Ti-based hydrogen storage electrode alloys were investigated systemically. Several key factors for example corrosion resistance, pulverization resistance and oxidation resistance were evaluated individually. The V-based solid solution phase has much lower anti-corrosion ability than C14 Laves phase in KOH solution, and the addition of Cr in V–Ti-based alloys can suppress the dissolution of the main hydrogen absorption elements of the V-based phase in the alkaline solution. During the charge/discharge cycling, the alloy particles crack or break into several pieces, which accelerates their corrosion/oxidation and increases the contact resistance of the alloy electrodes. Proper decreasing the Vickers hardness and enhancing the fracture toughness can increase the pulverization resistance of the alloy particles. The oxidation layer thickness on the alloy particle surface obviously increases during charge/discharge cycling. This deteriorates their electro-catalyst activation to the electrochemical reaction, and leads to a quick degradation. Therefore, enhancing the oxide resistance can obviously improve the cyclic stability of V–Ti-based hydrogen storage electrode alloys.

1. Introduction

Among all the hydrogen storage electrode alloys being developed today, rare earth based AB_5 type alloys have been commercialized successfully. Considering the somewhat low discharge capacity of AB_5 type alloys [1], usually less than 320 mAh g^{-1}, some new types of hydrogen storage electrode alloys with higher discharge capacity such as AB_3 type [2,3], V-based [4], Mg-based [5,6] and V–Ti-based [7] alloys were developed.

V–Ti-based multiphase hydrogen storage alloys, namely 'Laves phase related BCC solid solution', with high discharge capacities are extensively being investigated for the commercial usage as negative electrode for Ni/MH batteries [8–11]. This type of alloys mainly consist of a V-based solid solution BCC (body centered cubic) phase as the main hydrogen absorption phase and a network of TiNi BCC phase or C14 Laves phase as the secondary phase of electro-catalyst and micro-current collector. However, some drawbacks such as the high cost and poor cyclic stability prevent them from the practical application. Our previous work indicated that the proper substitution of Fe for Cr can effectively lower their price and improve the overall electrochemical properties [12]. But the poor cyclic stability of this type of alloys is still a serious problem for their commercial usage.

The cyclic stability of hydrogen storage electrode alloys is affected by many factors [13], and considerable studies have been carried out on the capacity degradation mechanisms of hydrogen storage electrode alloys. The results indicated that the capacity degradation of AB_5 type alloys was mainly caused by the oxidation/corrosion of active elements in alloys and the pulverization of alloy particles caused by the lattice expansion/contraction due to hydride formation/decomposition [14]. For Mg-based and V-based alloys, the dissolutions of Mg or V into the KOH solution were responsible for their capacity degradation [15,16]. For Ti-based AB_2 type alloys, the capacity degradation was attributed mainly to the deterioration of surface properties due to the formation of titanium-oxide on the surface of alloy particles [17].

In order to determine the degradation factors of the V–Ti-based hydrogen storage electrode alloys, Pan and co-workers [18–21] studied their degradation mechanisms during charge/discharge cycling in alkaline electrolyte extensively. And their results showed that the factors that affected the capacity degradation of V–Ti-based hydrogen storage electrode alloys could be divided into intrinsic factors and extrinsic factors. The oxidation/corrosion of the active components and the appearance of the irreversible hydrogen were two dominating intrinsic factors. The pulverization of the alloy particles during charge/discharge cycling was a key extrinsic factor. In practice, these two factors could not work independently. For example, the pulverization of the alloy particles accelerated the oxidation/corrosion of the active components.

* Corresponding author. Tel.: +86 574 8668 5097; fax: +86 574 8668 5702.
E-mail address: miaohe@nimte.ac.cn (H. Miao).

0925-8388/$ – see front matter © 2010 Elsevier B.V. All rights reserved.
doi:10.1016/j.jallcom.2010.08.132

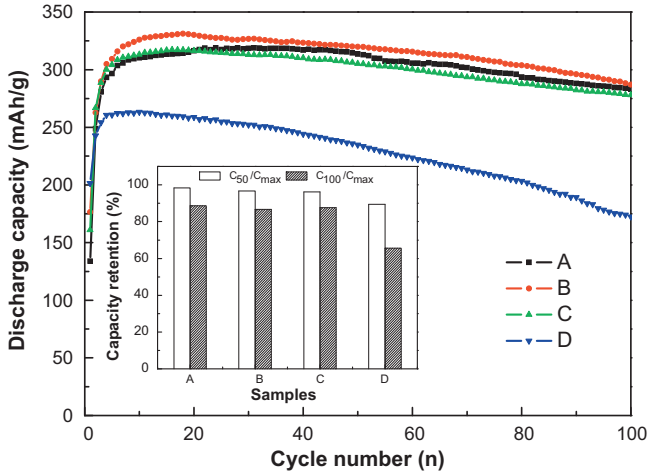

Fig. 1. Cyclic stability plots of alloy A, B, C and D at 303 K.

Recently, some studies indicated that proper annealing treatment [22] and the addition of Pd [23] or Ni [13] in the alloys could improve the cyclic stability of V–Ti-based hydrogen storage alloys effectively. But the further explanations on the mechanisms of improving the cyclic stability were not given in these papers. In this paper, based on our previous work, $Ti_{0.8}Zr_{0.2}V_{2.7}Mn_{0.5}Cr_{0.6}Ni_{1.25}Fe_{0.2}$ alloy anneal treated with water cooling [24], as-cast alloys of $Ti_{0.8}Zr_{0.2}V_{2.7}Mn_{0.5}Cr_{0.6}Ni_{1.15}Co_{0.1}Fe_{0.2}$ [21], $Ti_{0.8}Zr_{0.2}V_{2.7}Mn_{0.5}Cr_{0.4}Ni_{1.25}Fe_{0.4}$ [12] and $Ti_{0.8}Zr_{0.2}V_{2.7}Mn_{0.5}Ni_{1.25}Fe_{0.8}$ [12] were selected and named as A, B, C and D, respectively. And then the mechanisms of improving the cyclic stability of V–Ti-based hydrogen storage electrode alloys were systemically investigated.

2. Experimental

The preparations of alloy B, C and D were the same as reported in our previous study [12], and the details of the preparation of alloy A were described in Ref. [24]. The alloy samples were mechanically crushed and ground to powder of 300 mesh size ($\leq$50 μm) for X-ray diffraction (XRD) and the electrochemical measurements. XRD data of alloy C was collected by a step-scanning method using an ARL X-ray diffractometer with Cu Kα radiation in a power of 4 kV × 40 mA, and a step interval of 0.04° and a count time of 3 s per step were used. The microstructure of alloy C was observed by a FEI-SLRION scanning electron microscope (SEM) after the sample was mechanically polished and etched by a reagent of 10% HF, 10% HCl and 80% C_2H_5OH (by volume). Element distribution in the phases of alloy C was detected by energy dispersive spectroscopy (EDS) by using SEM.

The test electrodes were prepared by mixing 0.1 g alloy powder with 0.4 g carbonyl nickel powder and then cold pressing the mixture under a pressure of 800 MPa into a pellet with the diameter of 10 mm and thickness of about 1 mm. The cyclic stability measurements were performed in a half-cell consisting of a working electrode (MH electrode), a sintered $Ni(OH)_2$/NiOOH counter electrode and a Hg/HgO reference electrode. The electrolyte was a 6 M KOH solution, controlled at 30 ± 1 °C. The cycle life of the alloy electrodes was tested by charging the electrode at 100 m Ag^{-1} for 5 h followed by a 10 min break, and then discharging the electrode at 60 mA g^{-1} to the cut-off potential of −0.6 V vs. the Hg/HgO reference electrode. The cyclic stability of the alloy electrodes is evaluated by the retention of the discharge capacity after 100 charge/discharge cycles (C_{100}/C_{max}).

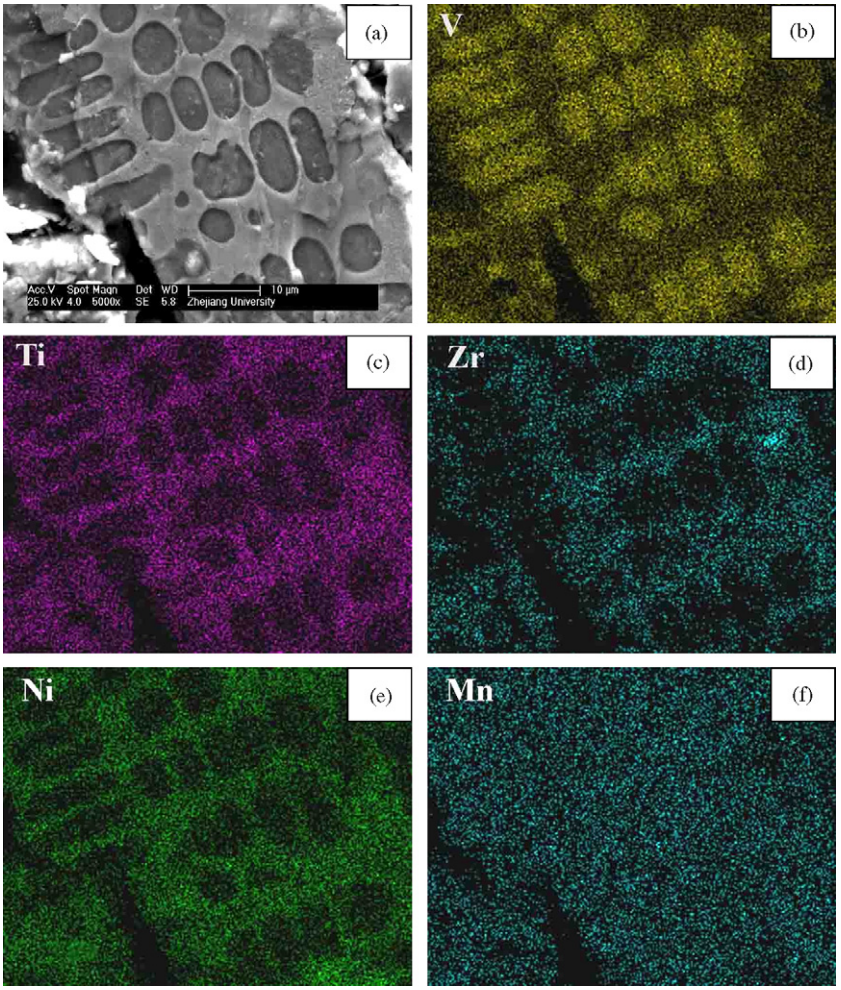

Fig. 2. EDS element maps of alloy C dipped in the 6 M KOH solution for 720 h stilly: (a) the detected area; (b) element V; (c) element Ti; (d) element Zr; (e) element Ni; (f) element Mn.

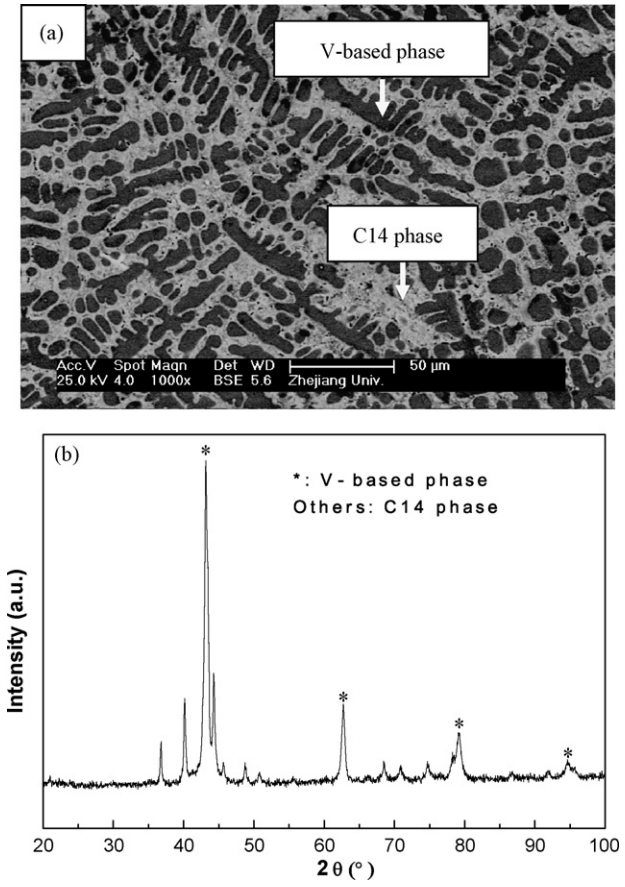

Fig. 3. Microstructure characters of alloy C: (a) SEM image; (b) XRD pattern.

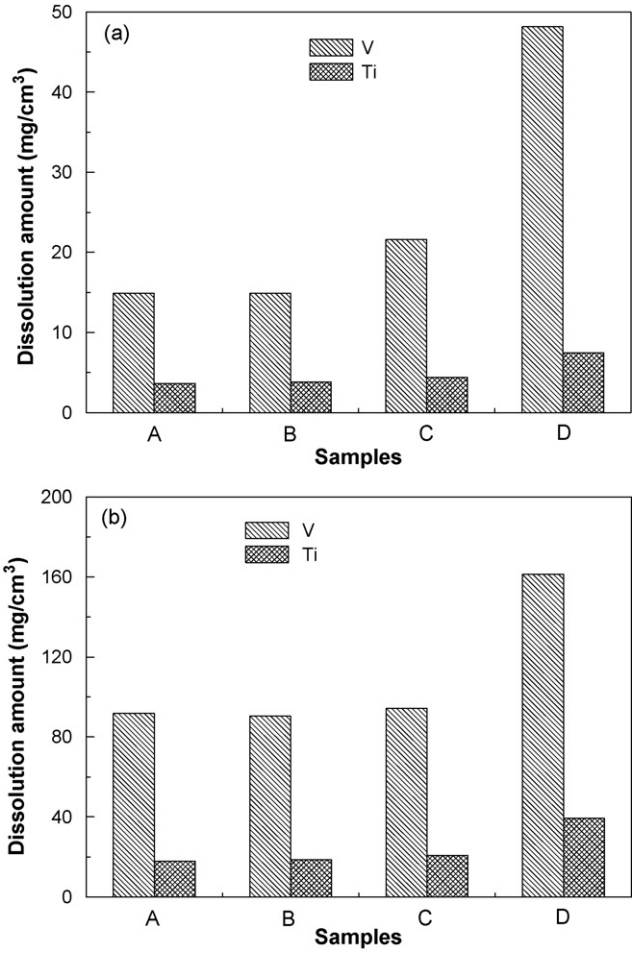

Fig. 4. Dissolution amounts of V and Ti of A, B, C and D alloys in the 6 M KOH solution: (a) after dipping for 1000 h stilly; (b) after 100 charge/discharge cycles (total time is about 1000 h).

To investigate the dissolution of V and Ti elements in the alkaline electrolyte after 100 charge/discharge cycles, the KOH solution was analyzed by a 721-type spectrophotometer. To investigate the pulverization extent of the alloy particles after 100 charge/discharge cycles, the morphology of the alloy particles was observed by SEM. To study the corrosion behaviors of this series of alloys, the pellets of alloy A, B, C and D were dipped into the 6 M KOH solution stilly for 720 or 1000 h, and then the morphology of the alloy particles and the dissolution amount of V and Ti were investigated by SEM and 721-type spectrophotometer, respectively. Element distribution in the alloy particles after the dipping process was detected by EDS by using SEM.

Toughness and hardness of alloy A, B, C and D was estimated by a Vickers indentation method, in which a diamond pyramid indenter and a load of 49 N were used. For Auger electron spectroscopy (AES) analysis, the test electrode was prepared by cold pressing 500 mg pure alloy power under a pressure of 800 MPa into a pellet of 10 mm diameter and about 1.5 mm thickness. AES depth profiles were measured for investigating the elemental distribution on the surface of the electrodes before cycling and after 100 charge/discharge cycles by using a PHI-550 type electron spectrometer with an electron beam at 3 kV and 10 μA. The electrode surface was sputtered with Ar^+ on an area of $1.5 \times 1.5\ mm^2$ at 4 kV and 15 mA, and the sputter rate was 2 nm/min.

Table 1
Compositions of the two phases of alloy C.

Samples	Phase	Composition (at.%)						
		Ti	Zr	V	Mn	Ni	Cr	Fe
Alloy C	C14	26.9	6.1	15.6	5.3	37.0	1.5	5.6
	bcc	5.0	0.5	61.0	9.1	8.0	7.8	8.6

3. Results and discussion

3.1. Cyclic stability

Fig. 1 shows the discharge capacity vs. cycle number of A, B, C and D alloy electrodes. In the present study, the cyclic stability can be evaluated by the retention of the discharge capacity after 100 charge/discharge cycles (C_{100}/C_{max}). From Fig. 1, it can be seen clearly that the values of C_{100}/C_{max} of alloy electrode A, B and C are almost same, which are in the range of 86.7–88.7%. Whereas, the value of C_{100}/C_{max} of alloy electrode D is 65.6%, which is about 22% lower than that of alloy electrode A, B and C.

Liu et al. reported [13] that the cyclic stability of the V–Ti-based electrode alloy was related to its corrosion resistance, pulverization resistance and oxidation resistance. The following section will further discuss the mechanisms of improving the cyclic stability of V–Ti-based hydrogen storage electrode alloys in terms of their corrosion behaviors, pulverization behaviors and oxidation behaviors individually.

3.2. Corrosion behaviors

Fig. 2 shows the SEM image and EDS element maps of alloy C dipped in the 6 M KOH solution for 720 h stilly. Obviously, some concaves can be found on the surface of this alloy. These concaves must belong to some phase of the alloy which has much lower corrosion resistance. In addition, EDS results indicate that this phase

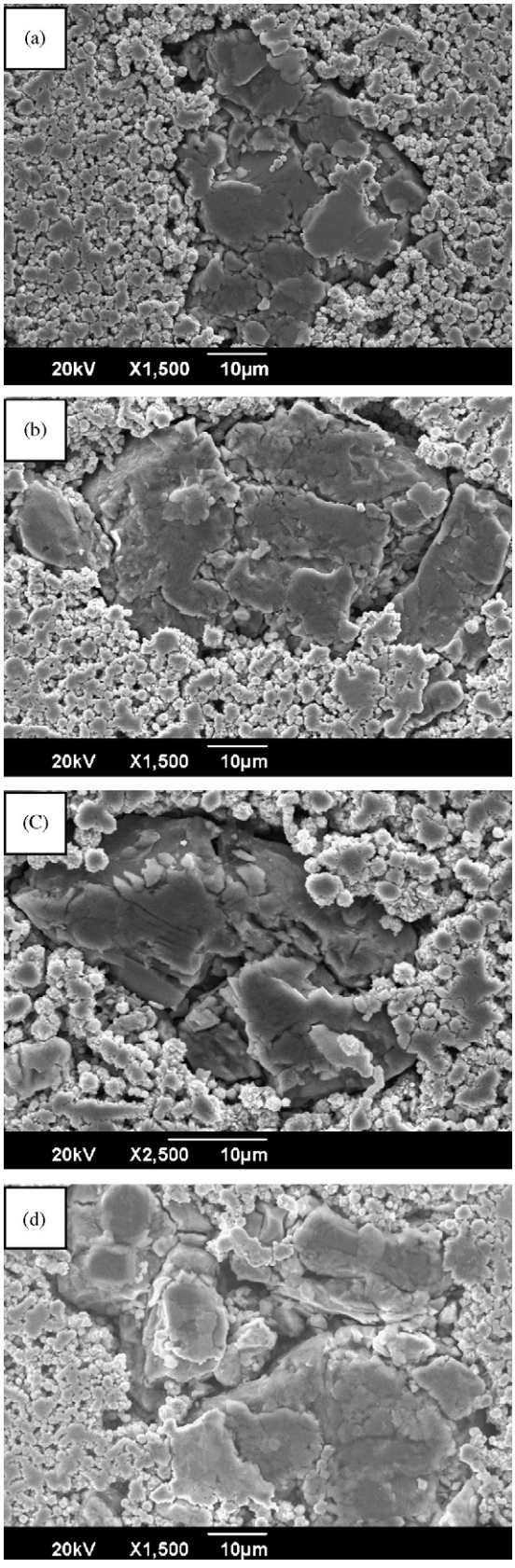

Fig. 5. SEM micrographs of A, B, C and D alloy particles after 100 charge/discharge cycles.

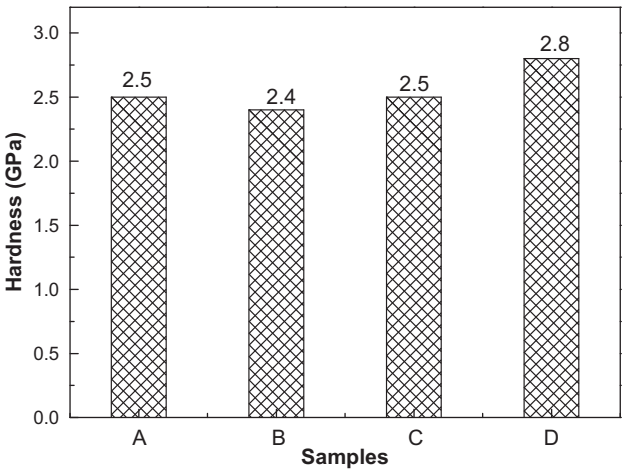

Fig. 6. Vickers hardness of A, B, C and D alloys.

(concaves) consists of much more V and less Ti, Zr and Ni than that of the other phase (the convexes). Fig. 3 shows the microstructure characters of alloy C. XRD result indicates that the alloy is composed of a C14 Laves phase with hexagonal structure and a V-based solid solution phase with a bcc structure. The C14 Laves phase is the light gray 3D interpenetrating structure, and the V-based solid solution phase is the dark gray dendritic structure. The compositions of the two phases are listed in Table 1. Apparently, much more V and less Ti, Zr and Ni in the V-based solid solution phase than in C14 Laves phase. Comparing the results obtained from Figs. 2 and 3 and Table 1, it can be concluded that the V-based phase becomes concave and the C14 Laves phase becomes convex during dipping process, which indicates that the V-based BCC phase has less corrosion resistant than the C14 Laves phase.

Fig. 4 shows the dissolution amounts of V and Ti of A, B, C and D alloys in the 6 M KOH solution after dipping for 1000 h stilly and 100 charge/discharge cycles (total time is about 1000 h). It can be seen from Fig. 4(a) that the dissolution amounts of V of A, B and C alloys are in the range of 9.9–14.4 mg/cm^3, whereas, the dissolution amount of V of alloy D reach 32.1 mg/cm^3 after dipping for 1000 h. This indicates that the corrosion resistances of alloy A, B and C are somewhat higher than that of alloy D. It was reported that the addition of Cr in the Laves phase alloys can effectively improve their cyclic stability due to the formation of Cr_2O_3 film on the alloy surface which can suppress the dissolution of the major components of the alloys into the KOH solution [25]. Moreover, for V–Ti-based alloys, a majority of Cr exists in V-based solid solution phase (Table 1), and this can further improve the anti-corrosion ability of this phase. For alloy D, no Cr existing may be one of the explanations for its low corrosion resistance in alkaline solution.

As can be seen from Fig. 4(b), the dissolution amounts of V of A, B and C alloys after 100 discharge/discharge cycles are in the range of 90.4–94.3 mg/cm^3, while the dissolution amounts of V of alloy D is 161.4 mg/cm^3. Apparently, the dissolution amounts of V of A, B and C alloys are less than that of alloy D after 100 discharge/discharge cycles. This tendency is almost same with that from Fig. 4(a). Moreover, comparing the results from Fig. 4(a) and (b), the dissolutions of V of all the alloys are accelerated due to the charge/discharge cycles which lead to the pulverization of the alloy particles. The following section will systemically discuss the pulverization behaviors of the alloy particles during charge/discharge cycling.

3.3. Pulverization behaviors

Fig. 5 shows the SEM micrographs of A, B, C and D alloy particles after 100 charge/discharge cycles. Obviously, some cracks appear

on the surface of A, B and C alloy particles, while D alloy particles break into several pieces after 100 charge/discharge cycles. This means that the pulverization resistance of alloy A, B and C is much higher than that of alloy D.

It was reported that the pulverization resistance of the hydrogen storage electrode alloys could be related to their hardness as well as fracture toughness [20,26,27]. As can be seen in Fig. 6, the Vickers Hardness values of A, B and C alloys are in the range of 2.4–2.5 GPa, while that of alloy D is 2.8 GPa. The alloy D is much harder than the other three. Fig. 7 displays the images of the Vickers indentation under the load of 49 N on the surface of A, B, C and D alloys. Certainly, the indentation size of alloys A, B and C is a little larger than that of alloy D. Moreover, there are very short indentation cracks in the A, B and C alloys, whereas, there are much longer indentation cracks in alloy D. It is no doubt that the fracture toughness values of alloy A, B and C are much higher than that of the alloy D.

It is well known that hydrogenation and dehydrogenation of hydrogen storage alloys result in a serious expansion and contraction of the hydrogen storage phases, respectively, and then the residual stress generates and accumulates during hydrogenation/dehydrogenation cycling [14]. When the residual stress accumulates to some extent, the particles of hydrogen storage alloys crack, and the pulverization behavior takes place. Tsukahara et al. [26] reported that the pulverization rate of V–Ti-based alloys could be closely related to its hardness, and a higher hardness caused a severer pulverization. Moreover, Yu et al. [27] indicated that enhancing the mechanical strength could effectively improve the anti-pulverization ability of the V-based solid solution alloys. So the poor anti-pulverization ability of alloy D can be attributed to its high hardness and low mechanical strength, such as the fracture toughness.

3.4. Oxidation behaviors

On the purpose of clarifying the correlation between the cyclic stability and oxidation resistance of this series of hydrogen storage electrode alloys, the elemental distributions on the surface of the electrode alloys were investigated by AES. The AES depth profiles of A, B, C and D alloy electrodes before cycling and after 100 charge/discharge cycles were displayed in Fig. 8. The content of oxygen decreases, while the content of vanadium increases gradually with the distance from the outer surface to the bulk of alloy electrodes. Then, the content of oxygen and vanadium keeps almost unchanged when the sputter time attains some value. The corresponding sputter distance can be related to the thickness of oxidation layer of the alloy electrodes.

For all the alloys, it can be seen obviously that the oxidation layers of the alloy electrodes after 100 cycles are much thicker than that before cycling, which means that the charge/discharge cycling accelerates the oxidation the alloy electrodes. For example, the oxidation layer thickness of the alloy A is 20 nm before cycling, and it increases to 90 nm after 100 charge/discharge cycles. Moreover, the oxidation layer thickness of alloy A, B and C, which is about 17–28 nm and 83–90 nm before cycling and after 100 cycles, respectively, is much thinner than that of alloy D, which is 46 and 124 nm before cycling and after 100 cycles, respectively. This result signifies that the anti-oxidation ability of alloy D is much weaker than that of alloy A, B and C. This can be related to its poor anti-pulverization ability. The oxide of the alloy electrode weakens its electro-catalysis activation to the electrode reaction, and results in the capacity degradation. So enhancing the anti-oxide ability is one of the effective methods for V–Ti-based hydrogen storage electrode alloys to improve their cyclic stability.

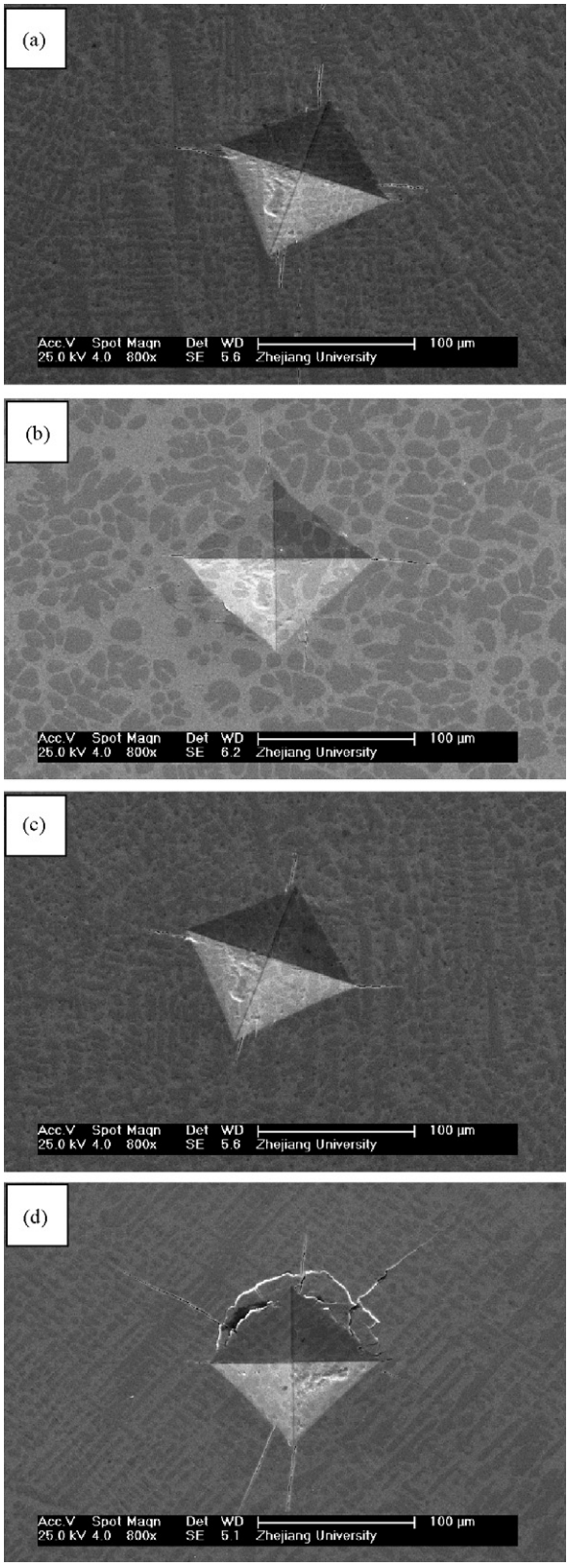

Fig. 7. Images of Vickers indentation of A, B, C and D alloys under a load of 49 N.

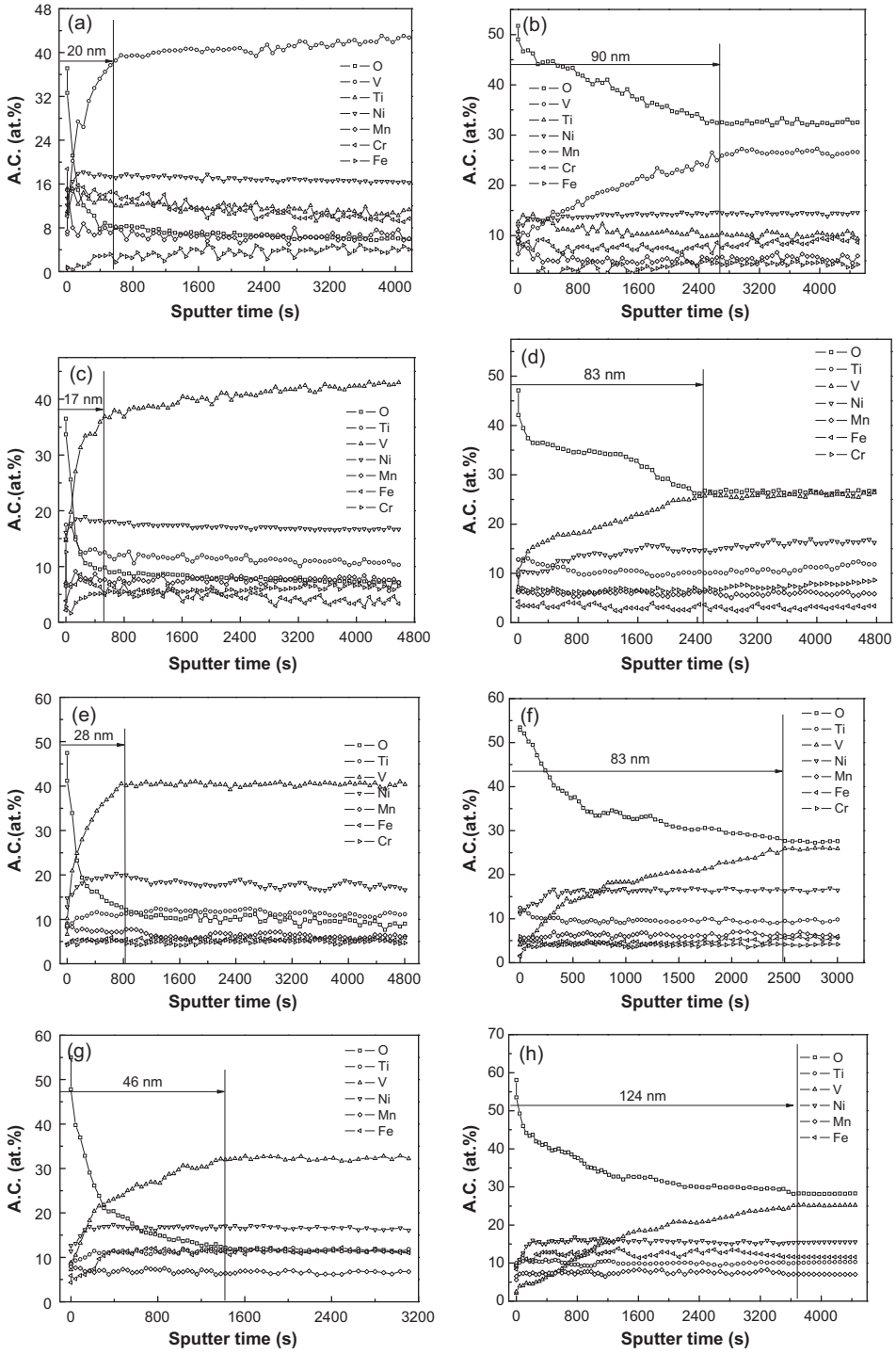

Fig. 8. AES depth profiles of A, B, C and D alloy electrode before cycling and after 100 charge/discharge cycles: before (a) and after 100 cycles (b) of alloy A; before (c) and after 100 cycles (d) of alloy B; before (e) and after 100 cycles (f) of alloy C; before (g) and after 100 cycles (h) of alloy D.

4. Conclusions

In this paper, the mechanisms of improving the cyclic stability of V–Ti-based hydrogen storage electrode alloys were investigated in terms of their corrosion behaviors, pulverization behaviors, and oxidation behaviors during charge/discharge cycling. And the following conclusions can be obtained:

a. For V–Ti-based alloys, the corrosion resistance of the V-based solid solution phase is much lower than that of C14 Laves phase. And the addition of Cr in the alloys, which distributes mostly in the V-based phase, can effectively increase the anti-corrosion ability of this series of alloys.
b. The pulverization of alloy D particles, which is very serious after 100 charge/discharge cycles, can be attributed to the high Vickers hardness and low fracture toughness. In addition, this pulverization behavior accelerates the corrosion and oxidation of the alloy electrodes. Decreasing the Vickers hardness and enhancing the fracture toughness can improve the cyclic stability of V–Ti-based alloys.

c. The nano-scale oxidation layer exists on the surface of the alloy particles before charge/discharge cycling, and this oxidation layer obviously increases after 100 charge/discharge cycles. Elevating the oxidation resistance is an effective method to improve the cyclic stability of the V–Ti-based alloys.

Acknowledgements

This work was financially supported in part by Ningbo Natural Science Foundation (2010A610147) and in part by China Postdoctoral Science Foundation (20090450745).

References

[1] J.J.G. Willems, K.H.J. Buschow, J. Less-Common Met. 129 (1987) 13.
[2] Y. Zhao, M.X. Gao, Y.F. Liu, L. Huang, H.G. Pan, J. Alloys Compd. 496 (2010) 454.
[3] X. Zhao, Q. Li, K. Chou, H. Liu, G. Lin, J. Alloys Compd. 473 (2009) 428.
[4] Y. Jia, L. Chen, X. Xiao, K. Yu, T. Ying, Y. Lei, Int. J. Hydrogen Energy 34 (2009) 7756.
[5] D. Vojtech, P. Guhlova, M. Mortanikova, P. Janik, J. Alloys Compd. 494 (2010) 456.
[6] M. Anik, J. Alloys Compd. 486 (2009) 109.
[7] K. Young, M.A. Fetcenko, F. Li, T. Ouchi, J. Koch, J. Alloys Compd. 468 (2009) 482.
[8] H. Iba, E. Akiba, J. Alloys Compd. 231 (1995) 508.
[9] M.X. Gao, H. Miao, Y. Zhao, Y.F. Liu, H.G. Pan, J. Alloys Compd. 484 (2009) 249.
[10] S.J. Qiu, H.L. Chu, Y. Zhang, D.L. Sun, X.Y. Song, L.X. Sun, F. Xu, J. Alloys Compd. 471 (2009) 453.
[11] R. Li, H.G. Pan, M.X. Gao, Y.F. Zhu, Y.F. Liu, Q.W. Jin, Y.Q. Lei, J. Alloys Compd. 373 (2004) 223.
[12] H. Miao, M.X. Gao, Y.F. Liu, Y. Lin, J.H. Wang, H.G. Pan, Int. J. Hydrogen Energy 32 (2007) 3947.
[13] Y.F. Liu, H.G. Pan, M.X. Gao, R. Li, Q.D. Wang, J. Phys. Chem. C 112 (2008) 16682.
[14] J.J.G. Willems, Philips J. Res. 39 (Suppl. 1) (1984) 1.
[15] Q. Tian, Y. Zhang, Y. Wu, J. Alloys Compd. 484 (2009) 763.
[16] X.B. Yu, Z. Wu, T.S. Huang, J. Alloys Compd. 476 (2009) 787.
[17] H.H. Lee, K.Y. Lee, J.Y. Lee, J. Alloys Compd. 260 (1997) 201.
[18] Y.F. Zhu, H.G. Pan, M.X. Gao, Y.F. Liu, R. Li, Y.Q. Lei, Q.D. Wang, Int. J. Hydrogen Energy 29 (2004) 313.
[19] H.G. Pan, Y.F. Zhu, M.X. Gao, Y.F. Liu, R. Li, Y.Q. Lei, Q.D. Wang, J. Alloys Compd. 364 (2004) 271.
[20] M.X. Gao, S.C. Zhang, H. Miao, Y.F. Liu, H.G. Pan, J. Alloys Compd. 489 (2010) 552.
[21] H. Miao, M.X. Gao, Y.F. Liu, D. Zhu, H.G. Pan, J. Power Sources 184 (2008) 627.
[22] Y.F. Zhu, H.G. Pan, M.X. Gao, Y.F. Liu, Q.D. Wang, J. Alloys Compd. 348 (2003) 301.
[23] Y.F. Liu, S.S. Zhang, R. Li, M.X. Gao, K. Zhong, H. Miao, H.G. Pan, Int. J. Hydrogen Energy 33 (2008) 728.
[24] M.X. Gao, H. Miao, Y.F. Liu, S.S. Zhang, J. Wang, H.G. Pan, J. Energy Storage Convers. 1 (2009) 61.
[25] S.R. Kim, K.Y. Lee, J.Y. Lee, J. Alloys Compd. 223 (1995) 22.
[26] M. Tsukahara, K. Takahashi, T. Mishima, A. Isomura, T. Sakai, J. Alloys Compd. 253–254 (1997) 583.
[27] J.S. Yu, S.M. Lee, K. Cho, J.Y. Lee, J. Electrochem. Soc. 147 (2000) 2013.